Realization of semi-integer mode plasmonic filters using sector-defected disk resonator

G. WAMG, Q. SHI, P. JI, F. CHEN*

School of Physics and Optoelectronic Engineering, Yangtze University, Jingzhou, 434023, China

A semi-integer mode plasmonic filter via a metal-insulator-metal (MIM) waveguide system is presented in this paper, the waveguide structure is composed of a nanodisk resonator with sector defect. Finite difference-time domain method (FDTD) is used to study the structure's transmission characteristics and magnetic field distributions. It is observed that the semi-integer mode can be excited in the sector-defected disk resonator. The positions and intensities of plasmonic resonant modes can be tuned by the angle of the sector defect, coupling distance, the refractive index of the nanodisk. The calculated maximum quality factors are 237.5, 381, and 286.5 respectively. Compared to the other related structure, the quality factor of the present sector-defected disk resonator structure is relatively excellent. The proposed plasmonic filter provides a basis for designing high quality factor filter and optical integrated circuits.

(Received November 15, 2021; accepted August 10, 2022)

Keywords: Surface plasmon polariton, Metal-insulator-metal, Sector defect, Plasmonic filter, Optical integrated circuits

1. Introduction

Surface plasmon polaritons (SPPs) are electromagnetic waves propagating along the surface of metal, which have been widely studied due to their strong confinement and light manipulation on nano scales[1-5]. In recent years, devices based on SPPs, such as the photonic integrated circuits, plasmonic filters, perfect plasmonic absorbers, plasmonic modulators, optical switches, plasmonic sensors, and modulators [6-12] are proposed and investigated. Among them, metal-insulator-metal waveguide (MIMW) or insulator-metal-insulator waveguide (IMIW) structures have been investigated widely due to their long propagation distance, and easy fabrication [13-14]. Plasmonic filters based on MIMW structure have been investigated by many groups, for example, MIM waveguide coupled with an improved nanodisk resonators[15], MIM waveguide coupled with a complementary split ring resonator for mode select optical filters [16]. plasmonic complementary aperture embedded in double-ring resonator for band-stop filter[17].

In the past decade, plasmonic filters with different configurations have been designed and investigated. For example, in 2017, Wen et al. reported and investigated a plasmonic multimode filter in MIM waveguide side coupled to a ring-groove joint resonator [18]. Li et al. proposed and studied filter effect based on a side coupled crossbeam square ring resonator [19]. Recently, Sun et al. investigated narrow band, low sideband plasmonic filter of asymmetric bi-layer metallic nanoslit arrays [20]. Zhang et al. proposed a tunable high-channel-count band-stop graphene plasmonic filters based on plasmon-induced transparency [21]. To achieve band-stop or band-pass filters, much attention has been focused on the wavelength-selection, on one hand, MIM waveguide side coupled to a resonator can realize a plasmonic band-stop filter. On the other hand, MIM waveguide directly coupled to a resonator can realize a

plasmonic band-pass filter.

Motivated by the work [16, 22], in this paper, a semi-integer mode plasmonic filter is presented in a compact plasmonic MIM waveguide system. The proposed structure is composed of two bus waveguides, a nanodisk resonator with a sector-defect. The introduction of sector defect inside the nanodisk resonator can produce semi-integer resonance mode due to symmetry breaking. Results show that the designed plasmonic structure can work as an excellent plasmonic filter, maximum quality factors about 237.5, 381, and 286.5 is obtained in the near-infrared band. The designed filter structure can be applied to the areas of optical integrated circuits and the design of high quality factor filters [23-26].

2. Model and theory

The proposed semi integer mode plasmonic filter is schematically depicted in Fig. 1, which consists of two MIM waveguides, and a sector-defected disk resonator is located between the two MIM waveguides with a coupling distance of *s*. The geometrical parameters are as follows: the radius of the sector-defected disk resonator is *R*, the angle of the the sector-defect is α. Due to the symmetry of the structure, the position of the sector-defect is defined as the angle (denoted by β) between the sector-defect and the y-aixs direction in the range of 0-90°. The width of the bus waveguide is w = 50 *nm*. The insulator in the nanodisk and the waveguide is set as air, the metal is assumed as silver, whose frequency-dependent complex relative permittivity can be characterized by the drude model [27-28]:

$$\varepsilon_m(\omega) = \varepsilon_\infty - \frac{\omega_p^2}{\omega^2 + i\omega\gamma_p} \tag{1}$$

where ε_∞ is the dielectric constant at the infinite frequency, ω_p and γ_p stand for the bulk plasmon frequencies and the electron collision, respectively, ω is the angular frequency of the incident light field. The parameters for silver can be set as ε_∞ = 3.7, ω_p = 9.1*ev* and γ_p = 0.018*ev* [29]. Two-dimensional simulation model is used since the structure in the z-direction is infinite. A TM-polarized plane wave propagates along the x direction, perfectly matched layers (PMLs) are applied in the x direction and y direction. The grid sizes in the x and y directions are chosen as 5×5*nm*.

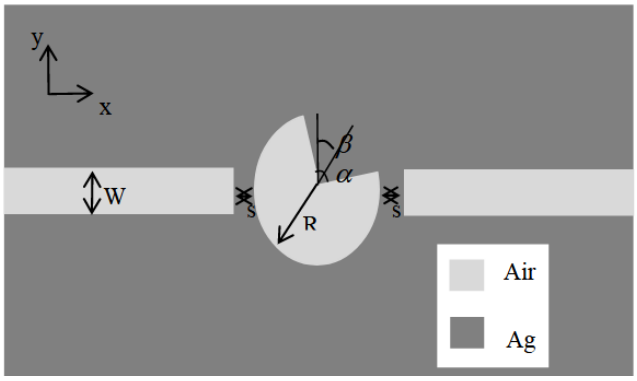

Fig. 1. The schematic diagram of the proposed plasmonic filter composed of a sector-defected disk resonator

Based on the standing wave theory, for the nanodisk resonator, the resonance wavelength of the nanidisk resonator is determined by the equation [30]:

$$k_i \frac{H_n^{(1)'}(k_m R)}{H_n^{(1)}(k_m R)} = k_m \frac{J_n^{'}(k_i R)}{J_n(k_i R)} \tag{2}$$

where R is the radius of the nanodisk resonator, $k_{i,m} = k(\varepsilon_{i,m})^{0.5}$ are the wave vectors in the nanodisk and metal, and $\varepsilon_i = 1$ is the relative permittivity of the air. n_{eff} can be described as: $n_{eff}(\omega) = (\varepsilon_{Ag}(\omega) + (\frac{k}{k_0})^2)^{1/2}$. k is the wave number. $H_n^{(1)}$ and $H_n^{(1)'}$ are the first kind Hankel function and its derivation with the order n, $J_n^{(1)}$ and $J_n^{(1)'}$ are the first kind Bessel function and its derivation with the order *n*.

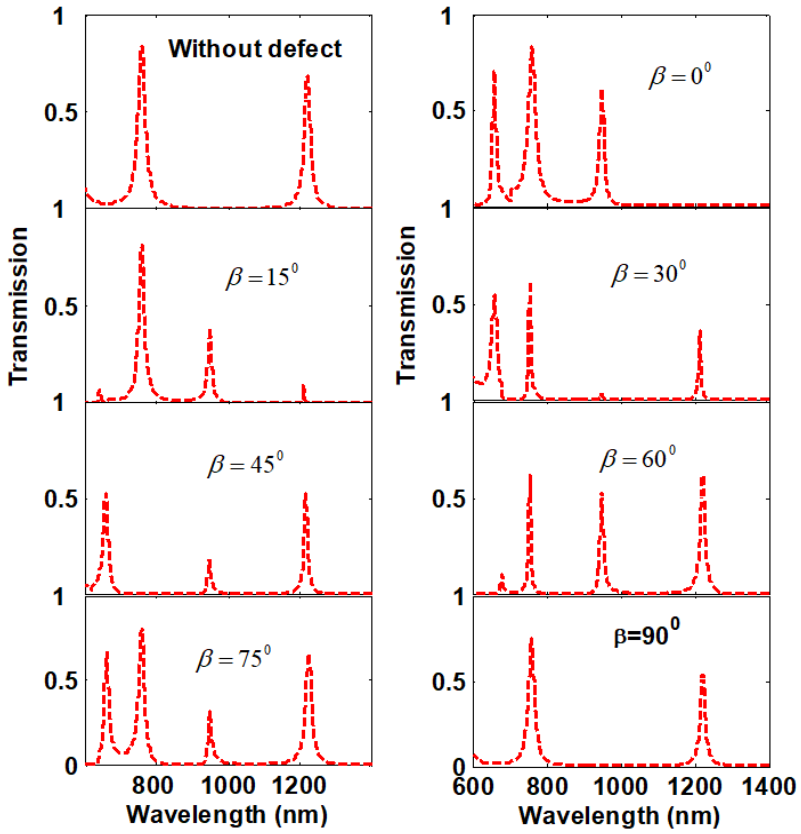

Fig. 2. The transmission spectra of the disk resonator without defect, and with a sector defect whose angle β from O° to 90°. (The geometrical parameters were set as w = 50 nm, s = 10 nm, R= 320 nm, and α = 8°) (color online)

According to the temporal coupled-mode theory [31], the transmittance can be calculated by:

$$T = \frac{\frac{1}{\tau_\omega^2}}{(\frac{1}{\tau_\omega} + \frac{1}{\tau_i})^2 + (\omega - \omega_0)^2} \qquad (3)$$

where ω_0 is the resonance frequency, ω is the frequency of the incident light, τ_ω^{-1} and τ_i^{-1} are the decay rate of the field induced by loss from the nanodisk resonator into the bus waveguide and the intrinsic loss inside the the nanodisk resonator, respectively. From Eq.(2) and (3), we can see that the resonance frequency ω_0 is determined by radius R and the wave vectors in the nanodisk, if the frequency of the incident light ω is equal to the resonance frequency ω_0, the incident light will pass through the structure, and if ω is far away from the resonance frequency ω_0, the incident light will be reflected back to in the input port. When τ_ω^{-1} is far bigger than τ_i^{-1}, the transmission peak ($\omega = \omega_0$) is close to unity.

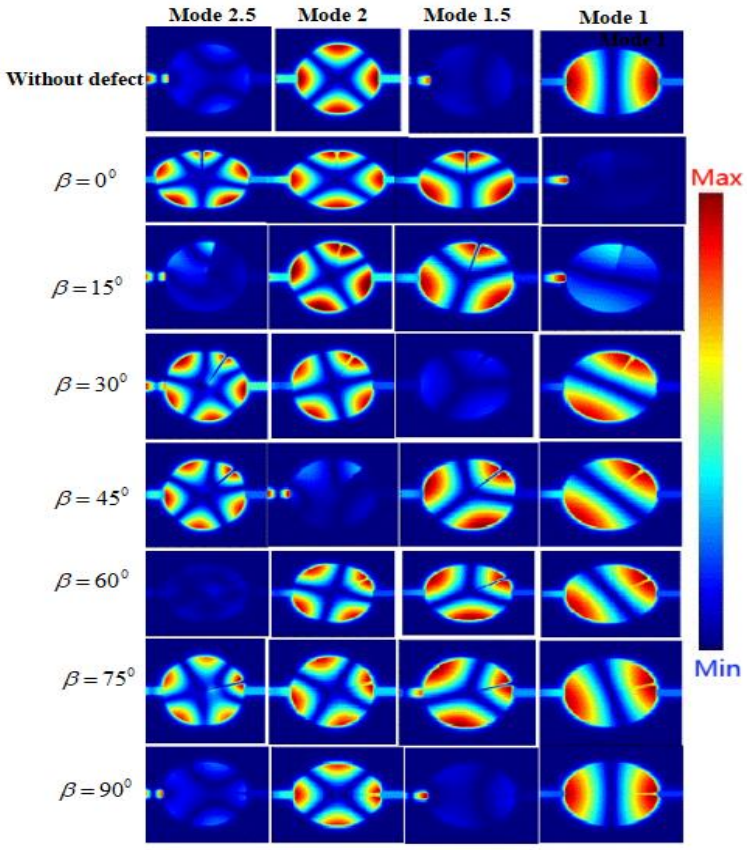

Fig. 3. Magnetic field patterns of the resonance modes (color online)

Fig. 2 shows the transmission spectra of the perfect disk resonator, and with a sector defect whose angle β from 0° to 90°, in the simulations, the parameters are $w = 50\ nm$, $s = 10\ nm$, $R = 320\ nm$, and $\alpha = 8°$. For a perfect nanodisk resonator, it can be seen two resonances modes (labeled by mode 1 and mode 2) of $\lambda_1 = 1222\ nm$, $\lambda_2 = 761\ nm$. The transmittance of the resonance peaks are 0.68, 0.82, respectively, the transmission spectrum exhibits a Lorentzian line shape. The transmittance peaks does not reach unity due to the propagation loss in the waveguide and the internal loss in the nanodisk resonator. It can also notice that mode 2 has a higher transmission than mode 1, this is because the resonant mode 2 has a larger τ_{ω}^{-1} than mode 1. From the magnetic field patterns, two and four antinodes can be found in the first line of Fig.3. When a sector-defecte is introduced in the nanodisk resonator from 0° to 90° with a step of 15°, as shown in Figs. 2 and 3, another two resonance modes labeled by mode 1.5 and mode 2.5 emerged in the transmission spectra. When $\beta = 0°$, the sector-defect is located in the antinode of the magnetic field pattern, the mode 1 is compressed while mode 2 remain unchanged. From the second line of Fig.3, it can be seen that mode 1.5, mode 2, mode 2.5 can pass through the bus waveguide, wile mode 1 is reflected back. When the sector-defect is located in $\beta = 15°$, 30°, 45°, 60°, 75°and 90°, the transmission spectra and the resonance mode distributions are shown in Fig 2 and 3. The transmittances of resonant modes with different positions of sector-defect is shown in Table 1, when $\beta = 15°$, mode 1 and mode 2.5 are suppressed, the transmittances are 0.37, 0.79 for mode 1.5 and mode 2. When $\beta = 30°$, mode 1.5 is suppressed, the transmittances are 0.36, 0.64, 0.54 for mode 1, mode 2, mode 2.5. When $\beta = 45°$, mode 2 is suppressed, the transmittances are 0.52, 0.16, 0.52 respectively. When $\beta = 60°$, mode 2.5 is suppressed, the transmittances are 0.62, 0.52, 0.6, respectively. When $\beta = 75°$, four modes are excited, the transmittances are 0.64, 0.32, 0.78, 0.64, respectively. When $\beta = 90°$, just like the perfect nanodisk resonator, mode 1 and mode 2 are excited. the transmittances are 0.55, 0.73,

respectively. The sector-defect can create more semi-integer resonant modes since the symmetry breaking of the nanodisk resonator.

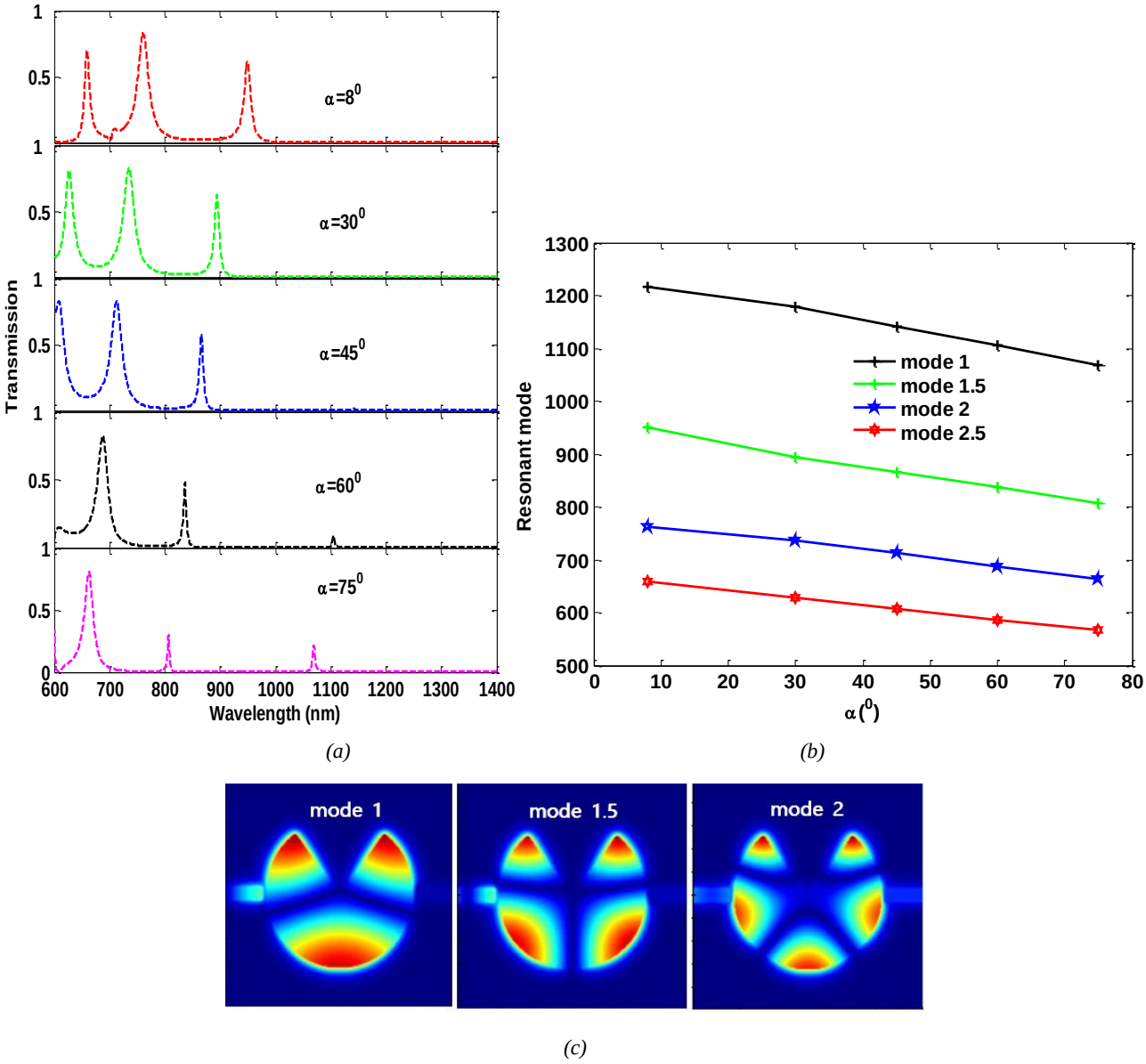

(a) *(b)*

(c)

Fig.4. (a) The transmission spectra of the plasmonic structure with different α *when* β = 0° *(b) Relationship between the resonance mode and* α *when* β = 0°. *(c) The magnetic field patterns of mode 1, mode 1.5, mode 2 when* α = 75° *(color online)*

Successively, we investigate the influence of the α on the transmission spectrum. As shown in Fig. 4 (a), when $\beta = 0^0$, the angle of sector defect increases from α = 8° to 30°, 45°, 60°, 75°, it can be seen that the resonant wavelengths are blue-shifted, the increasing α will change the resonant condition and the optical path in the defected disk resonator. The transmittance peaks are also changed with the increase of α, this is because the impedance matching condition is changed when varing α. The transmittance peak of mode 1.5 decreases while the transmittance peak of mode 1 increases. Fig. 4 (b) shows the relationship between the resonance mode and α, when α = 75° , mode 1 is appeared in the spectra. The magnetic field patterns of mode 1, mode 1.5, mode 2 when α = 75° are shown in Fig. 4 (c). Therefore, the resonant modes can be tuned by the angle of the sector defect.

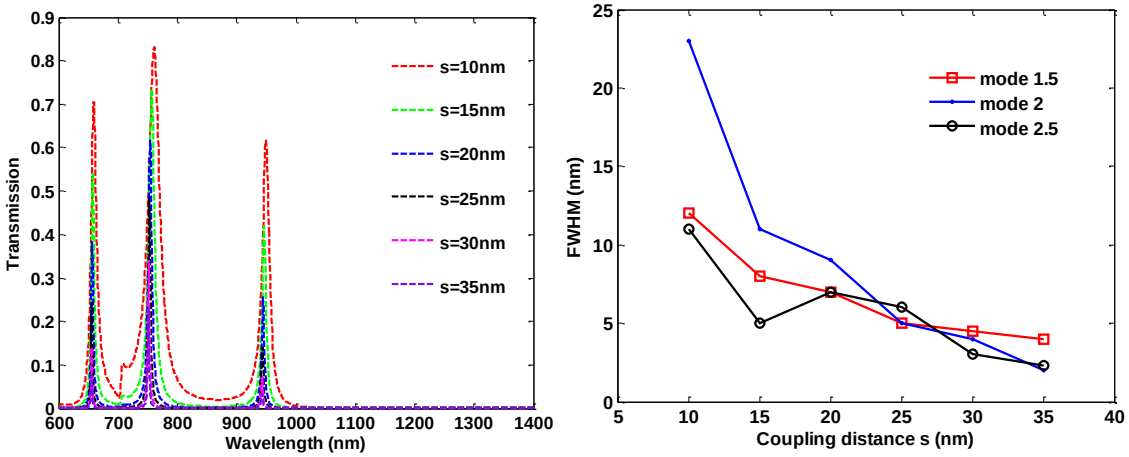

(a) *(b)*

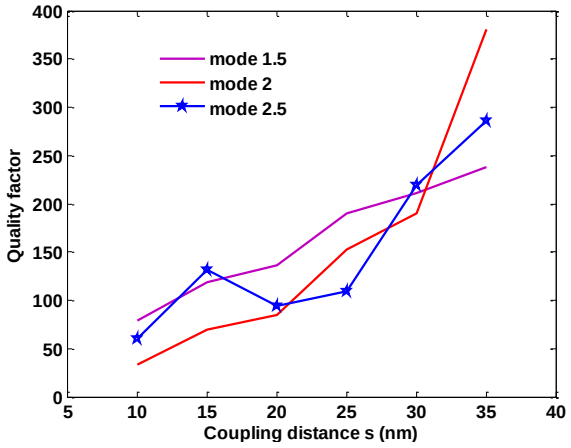

(c)

Fig. 5. (a)The transmission spectra of the plasmonic structure with different coupling distance s when α = 8°, β = 0°. (b) The relationship between coupling distance s and FWHM (c) The relationship between coupling distance s and Q (color online)

The effect of coupling distance s on the transmittance is studied in details. As shown in Fig. 5 (a), when the coupling distance s increases from s = 10 nm to 35 nm with a step of 5 nm, it can be seen that the resonant wavelengths are kept unchanged, but the transmittance peaks and FWHM are becoming smaller, the results are in line with the paper [32]. Fig. 5 (b) and (c) show the relationship between coupling distance s and FWHM, quality factor, when s increases from $s = 10\ nm$ to 35 nm with a step of 5 nm, it can be seen that the FWHM is becoming smaller, and the quality factors ($Q = \frac{\lambda_m}{FWHM}$) are becoming bigger. When coupling distance s is changed, the value of decay rate $1/\tau_i$ keeps unchanged since the dimension of nano-disk is unchanged. But the value of decay rate $1/\tau_\omega$ is decreasing, the transmission peak $T = (1/\tau_\omega)^2/(1/\tau_\omega + 1/\tau_i)^2$ will decrease. The full width at half maximum of the resonance spectrum $\Delta FWHM = 4\pi c(1/\tau_\omega + 1/\tau_i)/\omega_0^2$ is becoming smaller. Therefore, the bandwidths of resonant modes can be tuned by changing the coupling distance s.

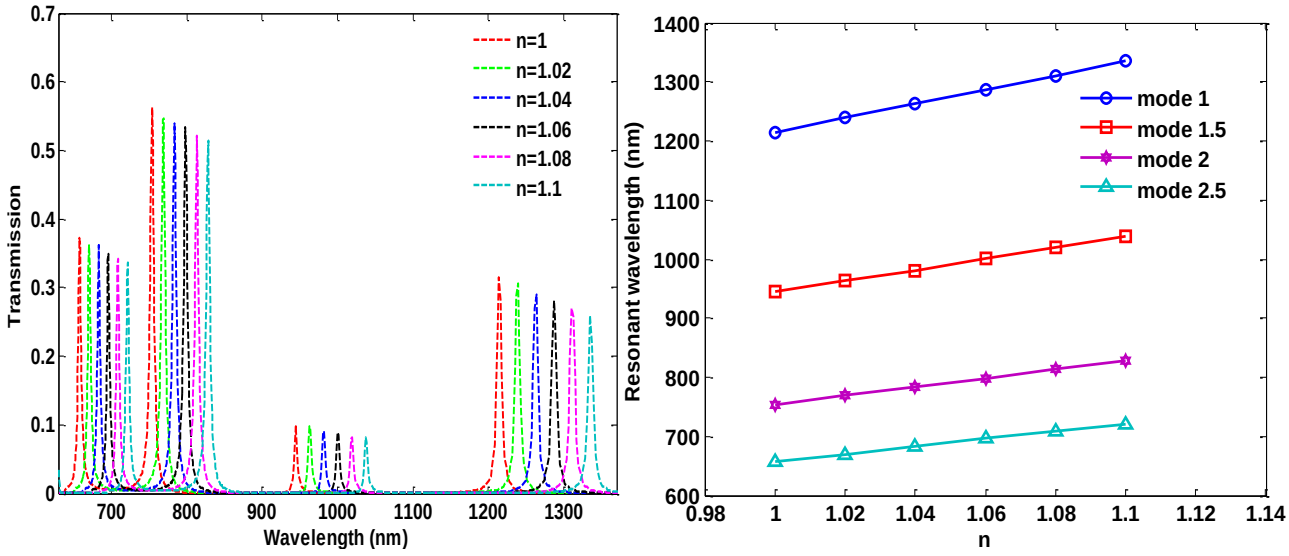

(a) *(b)*

Fig.6. (a) Transmission spectra with different n of the defect nanodisk resonator with β = 75° and s = 20 nm (b) The relationship between n and the resonant wavelength (color online)

Finally, we investigated the effect of refractive index on the transmission spectrum. According to Eq.(2), the resonant condition is related to the refractive index of the medium filled in the nanodisk resonator. Keeping β = 75°, s = 20 nm, α = 8°, R = 320 *nm*, w = 50 *nm*, when the refractive index is increased from 1 to 1.1 with a step of 0.02, the corresponding transmission spectra are shown in Fig. 6 (a), it can be seen that the resonant wavelengths have considerable red-shifts. Fig. 6 (b) shows the linear relationships between the refractive index and the resonant wavelength The FDTD simulation results are consistent with the resonant Eq.(2). Therefore, we can design the filter with different materials to meet the actual demand. Plasmonic filter can be realized in many structures, for example, cui et al. designed a multiple band rejection filter based on spoof surface plasmon polaritons [33]. To further evaluate the performance of the proposed plasmonic filter, resonator type, resonance wavelength, wavelength range, quality factor of our proposed plasmonic structure with other related structures are compared and the results are shown in Table 2. The quality factor of the present sector-defected disk resonator structure is relatively good compared to previous work. The proposed plasmonic filter can be produced by focused ion beam method, firstly, the focused ion baem is sputtered on the Ag film above the quartz substrate. The the waveguide resonator structure is patterned by controlling the position of the focused ion beam, with the development of micro-electro mechanical system and material science, the proposed semi-integer mode plasmonic filters will be produced.

Table 1. Transmittance of resonant modes with different positions of the sector-defected

β	Transmission			
	Mode 1	Mode 1.5	Mode 2	Mode 2.5
Without defect	0.68	0.00	0.82	0.00
0^0	0.00	0.59	0.82	0.68
15^0	0.08	0.37	0.79	0.06
30^0	0.36	0.02	0.64	0.54
45^0	0.52	0.16	0.00	0.52
60^0	0.62	0.52	0.60	0.09
75^0	0.64	0.32	0.78	0.64
90^0	0.55	0.00	0.73	0.00

Table 2. Comparisons between the proposed filters and other works

Ref	Resonator type	Resonance wavelength(nm)	Wavelength Range(nm)	Maximumquality factor
This work	Defected nanodisk	1222 948 761 660	600-1400	--- 237.5 381 286.5
26	Ring+square	1261	700-2000	140
34	Nanonotch structure	1300	500-1800	72.2
35	Hexagonal resonator	1205	1100-1500	17.7
36	Nanodisk	1500	750-2500	125

3. Conclusion

In conclusion, we have investigated by FDTD simulation a plasmonic filter based on a nanodisk resonator with sector defect. The influence of the geometrical size on the transmission characteristics is studied in details. Results show that resonances modes, transmittance peaks, and FWHM can be tuned by the geometrical parameters, such as the angle of the sector defect, coupling distance, the refractive index of the nanodisk. Based on the symmetry breaking, semi integer resonant modes (mode 1.5, 2.5) are produced. A maximum quality factor of about 381was obtained. The designed filter structure can be applied to the areas of optical integrated circuits and the design of high quality factor filters.

Acknowledgements

Supported by the Yangtze Fund for Youth Teams of Science and Technology Innovation（Grant No. 2015cqt03）. National Natural Science Foundation of China (Grant No. 11747091). Yangtze Fund for college students' innovation and entrepreneurship (Grant No. Yz2021280).

References

[1] S. Zhang, D. A. Genov, Y. Wang, M. Liu, X. Zhang, Phys. Rev. Lett **101**, 047401 (2008).

[2] C. Genet, T. W. Ebbesen, Nature **445**, 39 (2007).

[3] F. Chen, H. F. Zhang, L. H. Sun, J. J. Li, C. C. Yu, Opt. Laser. Technol **116**, 293 (2019).

[4] S. Xiao, T. Wang, T. Liu, C. Zhou, X. Jiang, J. Zhang, J. Phys. D: Appl. Phys. **53**, 503002 (2020).

[5] G. Wang, H. Lu, X. Liu, Y. Gong, Nanotechnology **23**, 444009 (2012).

[6] Q. Zhang, X. G. Huang, X. S. Lin, J. Tao, X. P. Jin, Opt. Express **17**, 7549 (2009).

[7] X. C. Yan, T. Wang, H. Xu, S. Y. Xiao, Y. J. Zhu, Y. B. Wang, Plasmonics **12**, 1449 (2017).

[8] M. Singh, S. K. Raghuwanshi, O. Prakash, IEEE Sens. J. **19**, 4039 (2019).

[9] B. Z, Wei, S. S. Jian, Opt. Commun. **402**, (662017).

[10] S. Khani, M. Dannaie, P. Rezaei, IET Optelectron. **13**, 161 (2019).

[11] B. Ni, X. S. Chen, L. J. Huang, J. Y. Ding, G. H. Li, W. Lu, Opt. Quant. Electron. **45**, 747 (2013).

[12] Y. Neo, T. Matsumoto, T. Watanabe, M. Tomita, H. Mimura, Opt. Express **24**, 26201 (2016).

[13] R. E. Haffar, A. Farkhsi, O. Mahboub, Applied Phys. A **126**, 486 (2020).

[14] S. L. Li, Y. Wang, R. Z. Jiao, L. L. Wang, G. Y. Duan, L. Yu, Opt. Express **25**, 3525 (2017).

[15] K. Shiva, D. Mohammad, R. Pejman, Opt. Commun. **42**, 147 (2018).

[16] Z. Iman, M. Amirreza, P. Tavakol. S. A. Mohammad, Opt. Express **20**, 7518 (2012).

[17] Z. C. Wei, X. M. Zhang, N. F. Zhong, X. P. Tan, X. P. Li, Y. B. Liu, F. Q. Wang, H. Y. Meng, R. S. Liang, Photon. Nanostruct. **23**, 45 (2017).

[18] K. H. Wen, Y. H. Hu, L. Chen, J. Y. Zhou, M. He, L. Lei, Z. M. Meng, Plasmonics **12**, 427 (2017).

[19] S. W Wang, Y. Li, Q. J. Xu, S. H. Li, Plasmonics **11**, 1291 (2016).

[20] H. Liu, Z. J. Sun, Opt. Express **29**, 13590 (2021).

[21] Z. R. Zhang, Y. Long, P. Y. Ma, H. Q. Li, Nanotechnology **28**, 475205 (2017).

[22] K. H. Wen, Y. H. Hu, L. Chen, L. Lei, Z. Guo, Applied Opt. **53**, 4158 (2014).

[23] F. Chen, D. Z. Yao, Opt. Commun. **369**, 72 (2016).

[24] Y. Zhang, Wenwei Liu, Zhancheng Li, Zhi Li, Hua Cheng, Shuqi Chen, Jianguo Tian, Opt. Lett. **43**, 1842 (2018).

[25] C. R. D. Galarreta et al., J. Opt. **22**, 114001 (2020).

[26] Z. H. Liu, Y. Gao, Opt. Commun. **501**, 127395 (2021)

[27] J. Zhu, N. Li, Opt. Express **28**, 19978 (2020).

[28] X. S. Lin, X. G. Huang, Opt. Lett **33**, 2874 (20080.

[29] P. B. Johnson, R. W. Christy, Phys. Rev. B **6**, 4370 (1972).

[30] S. L. Qiu, Y. P. Li, J. Opt. Soc. Am. B **26**, 1664 (2009).

[31] Q. Li, T. Wang, Y. K. Su, M. Yan, M. Qiu, Opt. Express **18**, 8367 (2018).

[32] H. Lu, X. M. Liu, D. Mao, L. R. Wang, Y. K. Gong, Opt. Express. **18**, 17922 (2010).

[33] A. Aziz, H. C. Zhang, P. H. He, W. X. Tang, R. Yi, H. A. Madni, T. J. Cui, J. Opt. **22**, 015001 (2020).

[34] J. Tao, X. G. Huang, S. H. Liu, J. Opt. Soc. Am. B **27**, 1430 (2010).

[35] W.A. Yun et al., Opt. Commun. **427**, 505 (2018).

[36] V. S. Fan, Appl. Phys. Lett. **87**, 131102 (2005).

*Corresponding author: chenfang@yangtzeu.edu.cn